




Article

Thermal Properties, Isothermal Decomposition by Direct Analysis in Real-Time-of-Flight Mass Spectrometry and Non Isothermal Crystallization Kinetics of Poly(Ethylene-co-Vinyl Alcohol)/Poly(ϵ -Caprolactone) Blend

Abdulaziz Ali Alghamdi , Hussain Alattas, Waseem Sharaf Saeed , Abdel-Basit Al-Odayni ,
Ahmed Yacine Badjah Hadj Ahmed, Ahmad Abdulaziz Al-Owais and Taieb Aouak *

Chemistry Department, College of Science, King Saud University, P.O. Box 2455, Riyadh 11451, Saudi Arabia; aalghamdia@ksu.edu.sa (A.A.A.); hussein_attas@hotmail.com (H.A.); aalodayni@ksu.edu.sa (A.-B.A.-O.); ybadjah@ksu.edu.sa (A.Y.B.H.A.); aowais@ksu.edu.sa (A.A.A.-O.)

* Correspondence: wsaeed@ksu.edu.sa (W.S.S.); taouak@ksu.edu.sa (T.A.)



Citation: Alghamdi, A.A.; Alattas, H.; Saeed, W.S.; Al-Odayni, A.-B.; Ahmed, A.Y.B.H.; Al-Owais, A.A.; Aouak, T. Thermal Properties, Isothermal Decomposition by Direct Analysis in Real-Time-of-Flight Mass Spectrometry and Non Isothermal Crystallization Kinetics of Poly(Ethylene-co-Vinyl Alcohol)/Poly(ϵ -Caprolactone) Blend. *Crystals* **2021**, *11*, 292. <https://doi.org/10.3390/cryst11030292>

Academic Editors: Assem Barakat and Alexander S. Novikov

Received: 27 February 2021

Accepted: 14 March 2021

Published: 16 March 2021

Publisher's Note: MDPI stays neutral with regard to jurisdictional claims in published maps and institutional affiliations.



Copyright: © 2021 by the authors. Licensee MDPI, Basel, Switzerland. This article is an open access article distributed under the terms and conditions of the Creative Commons Attribution (CC BY) license (<https://creativecommons.org/licenses/by/4.0/>).

Abstract: A series of poly(ethylene-co-vinyl alcohol)/poly(ϵ -caprolactone) blends with different compositions were prepared using solvent casting. The miscibility of this pair of polymers was investigated using differential scanning calorimetry (DSC), and proved by a negative Flory interaction parameter value calculated from the Nishi–Wang equation. The miscibility of this blend was also confirmed by scanning electronic microscopy (SEM). The thermal behaviors of the obtained materials were investigated by DSC, thermogravimetric analysis, and direct analysis in real-time-time-of-flight mass spectrometry and the results obtained were very relevant. Furthermore, the crystalline properties of the obtained materials were studied by DSC and X-ray diffraction where the Ozawa approach was adopted to investigate the non-isothermal crystallization kinetics. The results obtained revealed that this approach described the crystallization process well.

Keywords: poly(ethylene-co-vinyl alcohol)/poly(ϵ -caprolactone) blend; non-isothermal crystallization kinetics; thermal decomposition; direct analysis in real-time-time-of-flight mass spectrometry; thermal gravimetry analysis

1. Introduction

Many systems, which were based on the chemical combination of different monomers by random, block, and graft copolymerization, have been developed to improve the properties of polymers over the years [1–4]. The development and commercialization of new polymers are extremely expensive and generally require many years. However, employing a process that is based on polymer blends, which are inexpensive and easy to process, often reduces the production time and cost. This approach is also associated with shortcomings and has not been developed as rapidly as expected, partly because most physical blends of different high molecular weight polymers are quite immiscible [5–8]. Put differently, when mixed, the blend components will likely be separated into phases predominantly containing their respective kinds. This characteristic, combined with the generally low physical forces of attraction across the phase boundaries, usually imparts immiscible blend systems with poor mechanical properties. Despite this shortcoming, different physical blend systems have been commercialized, as will be discussed subsequently.

Poly(ϵ -caprolactone) (PCL), which is also called a Shapelock (US) or polymorph (UK), is a non-hazardous semicrystalline polymer that can be readily shaped by hand because of its low melting point (60 °C). Furthermore, this polymer can be decomposed by the hydrolysis of the ester linkages in its backbone under physiological conditions [8]. One of the principal routes for preparing this polymer is the ring-opening polymerization of ϵ -caprolactone in the presence of stannous octoate as the catalyst [9]. Furthermore,

the competitive viscoelastic and rheological properties of PCL enormously facilitate the manufacturing and handling of many polyesters into a wide range of implants and other devices [10–14]. This biodegradable and biocompatible polymer, which is approved by the US Food and Drug Administration and prepared by relatively inexpensive production routes, offers a promising basis for its utilization as long-term degradable implants. This polymer can be physicochemically manipulated according to specific anatomy sites to control the biodegradation process [15,16].

Furthermore, poly(ethylene-co-vinyl alcohol) (E-VAL) is a semicrystalline, biodegradable [17], biocompatible [18,19] copolymer that possesses excellent mechanical and gas barrier properties. Because of its double hydrophilic/hydrophobic character, this copolymer can be controlled through its composition of hydrophobic/hydrophilic comonomers, thereby favoring its application, such as tissue engineering, in the biomedical field through the hydrophilic character of the cells [20]. This copolymer is synthesized by the polymerization of ethylene with vinylacetate to yield poly(ethylene-co-vinylacetate), followed by the hydrolysis of the acetate substituent. Moreover, only a few investigations have been reported regarding the application of this copolymer in the biomedical domain. It is well known that certain properties of semicrystalline polymers are directly related to the dynamic behavior of the crystallization of a polymer [21,22]. Generally, a polymer can crystallize under isothermal or non-isothermal conditions upon heat treatment. The relevant kinetic behaviors are generally studied to elucidate the mechanism by which crystallization evolves in polymer materials. The kinetics of isothermal crystallization is widely applied to describe the evolution of a crystalline system in the polymer matrix [23–25]. However, some studies have focused on the non-isothermal crystallization of polymers through their processes, thereby reflecting the industrial conditions [26–28]. According to the literature, regarding the kinetics of isothermal crystallization, many models have been developed, although only some of them (Jeziorny [29], Ziabocki [30]), and Ozawa [31] are suitable for describing non-isothermal kinetics. To properly control the rate of crystallization and obtain the desired physical and mechanical properties of a material, kinetic studies via suitable mathematical models must be conducted [32]. The competitive viscoelastic and rheological properties of PCL and E-VAL greatly facilitate their manufacture and handling in a wide range of implants and other devices. However, these accessories have been developed on an industrial scale primarily via thermal molding under certain heating temperature and pressure conditions. Therefore, a study of the thermal stability of these materials is required.

In this work, a series of polymer blends involving PCL and E-VAL with different compositions were prepared via the solvent casting route, after which the crystalline and thermal properties of the resulting materials were studied. To achieve this, differential scanning calorimetry (DSC) analysis was employed to characterize the miscibility of this pair of polymers and study the non-isothermal crystallization kinetics of the obtained material. Therein, the Ozawa model was applied to determine the different crystallization parameters. Furthermore, thermogravimetric analysis/differential thermal analyses (TGA/TDA) was conducted to study the thermal stability of the obtained material and the nature of the resulting fragments from the thermal decomposition of the blends.

2. Materials and Methods

2.1. Materials

E-VAL (27% ethylene) and PCL ($\overline{M}_w = 45,000 \text{ g mol}^{-1}$) was supplied by Sigma-Aldrich (Schnelldorf, Germany). Dimethylformamide (DMF) (purity, 98%) was purchased from Panreac (Chicago, IL, USA). These chemicals were utilized without prior purification.

2.2. Blend Preparation

The E-VAL/PCL blend was prepared by the solution casting method. The polymer and copolymer were dissolved separately in DMF in a 50 mL Erlenmeyer flask at 80 °C, with stirring until complete dissolution was achieved, as observed by the formations of viscous

solutions. Thereafter, the two solutions were mixed with continuous stirring to form an E-VAL/PCL/DMF ternary solution. To obtain a film sample with perfectly homogeneous thickness, the solution was poured into a Teflon petri dish, after which they were all carefully deposited horizontally on a square Styrofoam plate, floating on the surface of a crystallizer that was filled with water and kept to dry for 48 h at ambient temperature. To extract the residual solvent that was crusted on the obtained film, the Teflon plate containing the polymeric material was vacuum-dried for 24 h at 60 °C. Furthermore, a series of E-VAL/PCL blends containing 10, 25, 50, 75, and 90 wt% E-VAL was prepared by the same method, and Table 1 presents the experimental conditions.

Table 1. Preparation conditions of the E-VAL/PCL blends in DMF.

Sample	E-VAL:PCL (wt%)	E-VAL (g)	PCL (g)
E-VAL	100:0	10.0	0
E-VAL/PCL90	90:10	9.0	1.0
E-VAL/PCL75	75:25	7.5	2.5
E-VAL/PCL50	50:50	5.0	5.0
E-VAL/PCL25	25:75	2.5	7.5
E-VAL/PCL10	10:90	1.0	9.0
PCL	0:100	0	10

2.3. Characterization

The polymer, copolymer, and their blends were characterized by different techniques. The X-ray diffraction (XRD) patterns of the E-VAL copolymer, PCL homopolymer, and their blends were recorded on a Rigaku D_{max} 2000 X-ray diffractometer that was equipped with a Cu anode tube at a voltage and generator current of 40 kV and 100 mA, respectively. Furthermore, the diffraction angle was in the range of 0–80 two theta. The samples were utilized as thin films, although the pure naphthalene sample was analyzed as powder microparticles. Surface morphology analyses of dried samples were performed on a Jeol JSM-6360LV scanning electron microscope (SEM) (Japan) at an accelerating voltage of 20 kV. The surface of samples was first sputter-coated with a thin layer of gold and then observed at a magnification range of 5000×. The DSC thermograms were obtained by a Shimadzu DSC-60 system, which was previously calibrated with indium. Additionally, 8–10 mg of the polymer sample was packed in aluminum DSC pans before they were placed in the DSC cell. The samples were heated from 30 °C to 200 °C at heating rates of 5, 7, 10, and 20 °C min^{−1} in nitrogen gas and kept at 200 °C for 10 min to destroy any nucleus that might act as a crystal seed. In the cooling mode, the samples were cooled to 50 °C at cooling rates of 5, 7, 10, 15, and 20 °C min^{−1}. For a uniform thermal history of all the samples, the data were obtained from the second scan runs of all the samples. No degradation phenomena were observed in all the DSC thermograms of E-VAL, PCL, and their blends. Noting that the T_g value was taken as the midpoint of the heat capacity change with temperature and the T_m and T_c at the top of the melting and crystallization changes with temperature, respectively. The TGA/DTA measurements were conducted on a Shimadzu TGA-60 system in dynamic nitrogen gas. Afterward, 4–10 mg of the polymer or copolymers was carefully loaded into the TGA aluminum pan and heated from 25 °C to 600 °C at a heating rate of 20 °C min^{−1}. The isothermal decomposition was detected by an Accu-time-of-flight (ToF) LC-plus JMS-T100 LP mass spectrometer (JEOL, Tokyo, Japan) that was equipped with direct analysis in real-time (DART) ion source (IonSense, Saugus, MA, USA) without any prior preparation of the sample. The volatile components of the extract were evaporated from a stream of helium that was heated at 350 °C, after which they were ionized by the excited metastable helium atoms before entering the ion source of the ToF mass spectrometer. In the positive ionization mode, each molecule was transformed into a protonated ion [M + H]⁺ or a non-protonated radical molecular ion [M⁺]. Since the ionization process was considered “soft,” only a little or no fragmentation occurred, such that each peak in the spectrum corresponded to a given compound. The high-resolution

mass spectra were recorded using the following experimental conditions: needle voltage: 3000 V, helium flow-rate: 0.5 L/min., detector voltage: 2200 V. The mass calibration was achieved using a mixture of standard polyethylene glycols PEG 200 and PEG 600. The mass spectra were recorded in the range 50 to 1000 Da, with a mass resolution between 4800 and 5450. The spectral data were stored and processed using Mass Center software. The surface morphology of the PE-co-VAL, PCL, and PE-co-VAC dried films, which were coated with a gold grid, was analyzed by field emission scanning electron microscopy (JEOL-JSM-2100F scanning electron microscope at accelerating voltage of 15 kV). The samples were first sputter-coated with a thin layer of gold before they were observed at a magnification range of 300–3000 \times .

3. Results

3.1. Miscibility

The miscibility of the E-VAL/PCL mixture with different compositions was recently proven by DSC and confirmed by Fourier-transform infrared (FTIR) analysis in our previous study [33]. The DSC analysis revealed the presence of a single T_g in the thermograms of the blends and its negative deviation from that of the ideal, and these indicated the interaction between the chains of different natures. The comparison of the FTIR spectra of the blends with their components revealed the presence of hydrogen bonds, thereby confirming the interaction of the two different polymers.

3.2. SEM Analysis

Figure 1 shows the SEM micrographs of the surface morphology of E-VAL, PCL, and E-VAL/PCL blends containing 25, 50, 75, and 90 wt% of E-VAL content. A homogeneous and smooth surface was observed in the micrographs of the E-VAL and PCL components. The SEM micrographs of the blends also showed smooth and uniform monophasic surface morphologies comparable to those of pure E-VAL and PCL devoid of any stress could be reflecting the repulsion forces causing the immiscibility. Noting that, an immiscible blend shows dull and heterogenic surfaces, proving the existence of stress resulting from the contraction of each constituent due to the electrostatic repulsion forces indicating the non-miscibility. The ripples or the wrinkles seen in photos of some samples probably resulted from bloating due to the evaporation of residual DMF during the vacuum drying period at 60 °C. Under these conditions, the vapor released lifts the film and then deposits it on the Teflon plate after the total evaporation of the solvent.

3.3. DSC Analysis

3.3.1. Glass Transition and Melting Temperature

The DSC thermograms of the E-VAL/PCL blends and their pure components revealed T_g and the apparent T_m (T_m^{app}), as presented in Table 2. According to the T_g values of the blend, regarding all the investigated compositions, the presence of only one transition temperature, which was localized between those of their pure components, indicated the miscible behavior of this pair of polymers in their amorphous forms. The T_g value of PCL shifted toward higher temperatures when the E-VAL content of the blend increased. According to Qui et al. [34], the appearance of a single T_g for the blend indicated the full miscibility on a 20–40 nm scale.

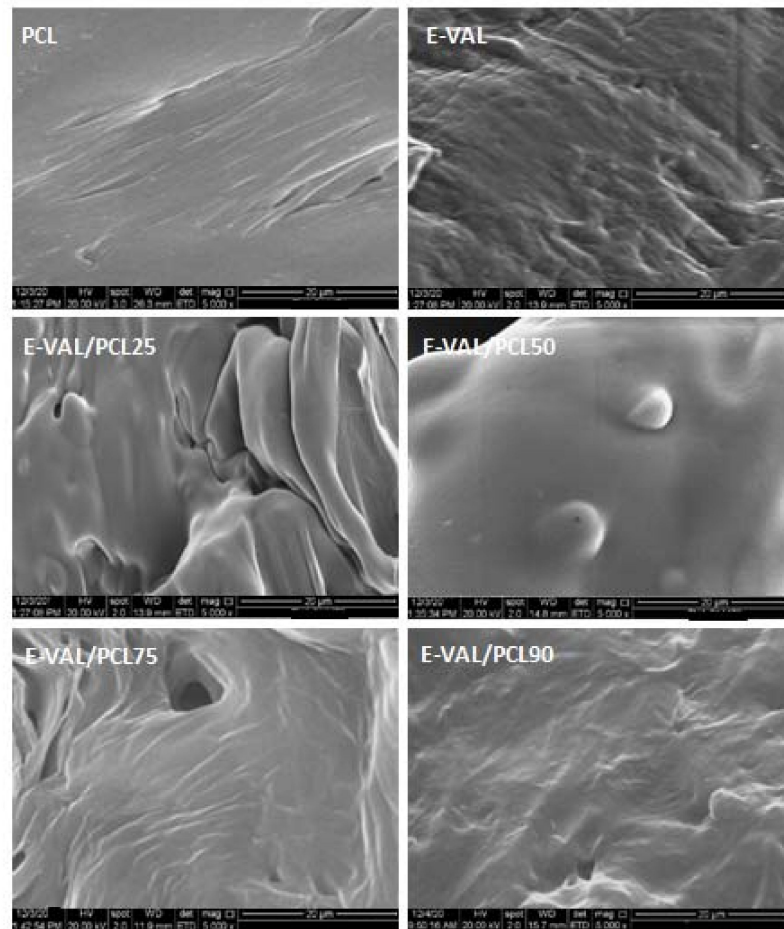


Figure 1. SEM micrographs of surface morphologies of E-VAL/PCL blends and their pure polymer components.

Table 2. Comparative data of the E-VAL/PCL blend with different compositions, obtained by DSC.

Blend System	PCL			E-VAL	
	T_g (°C)	T_m^{ap} (°C)	ΔH_m (J·g ⁻¹)	T_m^{ap} (°C)	ΔH_m (J·g ⁻¹)
E-VAL	60	-	-	183	73.70
E-VAL/PCL90	39	52	8.34	180	47.83
E-VAL/PCL75	17	56	14.18	178	31.32
E-VAL/PCL50	-12	67	45.46	177	27.02
E-VAL/PCL25	-33	65	69.19	175	24.57
E-VAL/PCL10	-53	64	73.12	167	19.65
PCL	-59	62	75.1	-	-

$\Delta H_m = 72.5$ J/g for E-VAL32% [35].

Two melting temperatures were observed in each thermogram. They were attributed to each constituent in the blend in which T_m^{ap} of E-VAL shifted moderately toward the low temperatures (from 183 °C to 167 °C), whereas that of PCL passed by a maximum of 67 °C when the composition was 50 wt%. The decrease in T_m of a semicrystalline polymer in the blend was caused by the thermodynamic interactions between the two different polymeric chains. According to the Flory–Huggins theory [36,37], a miscible blend is characterized by the magnitude of the reduction in T_m , which allows the assumption of the value of the interaction energy involved. T_m of a polymer is generally affected by thermodynamic factors and morphological parameters, especially the thickness of the crystal. It was also revealed from the data in Table 3 that the heat of fusion (ΔH_m), which was attributed to PCL in the blend, increased significantly with the E-VAL content, whereas that of E-VAL

similarly decreased. This appeared to be directly related to the degree of depression in the crystallinity of each component as the concentration of the other increased.

Table 3. Parameters of the Hoffman–Weeks plot for E-VAL in the E-VAL/PCL blends.

System	φ_{E-VAL}	$(\varphi_{E-VAL}^2) \times 10^2$	T_m^o (°C)	T_c (°C)	η
E-VAL	1.0	100	186	157	0.24
E-VAL/PCL90	0.895	80.10	183	154	0.17
E-VAL/PCL75	0.740	54.76	181	152	0.14
E-VAL/PCL50	0.487	23.72	176	150	0.14
E-VAL/PCL25	0.210	4.41	175	148	0.11
E-VAL/PCL10	0.095	0.90	173	145	0.11

Regarding the E-VAL/PCL blends, T_m^o .

To dissociate the thermodynamic effects on the decrease in T_m from the morphological parameters, we applied the equilibrium melting point (T_m^o) data. According to the Hoffman–Weeks approach [38], T_m^o is given by Equation (1):

$$T_m^{ap} = \eta T_c + (1 - \eta) T_m^o \quad (1)$$

This method is based on the isothermal crystallization of the polymer at different T_c , as displayed in Figure 2 for the pure components and blends containing equal amounts of each constituent, and the plot of the variations in T_m^{ap} with T_c . Moreover, T_m^o and η were obtained from the intercept of the straight line, $T_m^{ap} = T_c$, and the slope of the Hoffman–Weeks plot (Figure 3), respectively. According to the same authors, the value of η varied between zero and one and could be considered as a parameter for evaluating the stability of crystals undergoing melting. Indeed, $\eta = 0$ indicates that the crystals are perfectly stable, so that $T_m^{ap} = T_m^o$ at all the crystallization temperatures. Conversely, $\eta = 1$ represents intrinsically unstable crystals. Table 3 lists the η and T_m^o values of the E-VAL and E-VAL/PCL blends with different compositions. As shown in these data, T_m^o of E-VAL was observed at 186 °C, which agreed with the result in the literature (187 °C) [39].

Regarding the E-VAL/PCL blends T_m^o of the E-VAL phase decreased with the PCL content to reach a minimum of 173 °C when the PCL content of the blend was 10 wt%. In other terms, the maximum extent of this T_m depression in the E-VAL/PCL10 blend was 13 °C. Generally, the η values of E-VAL in its blend (0.24–0.11) were relatively small, thereby revealing the stability of the E-VAL crystals in the blend. This parameter decreased slowly as the PCL content of the blend increased, practically losing half when the concentration of PCL in the blend was 10%. This suggests that the stability of the E-VAL crystals increased relatively, i.e., their lamellar thicknesses increased, when blended with PCL. This fact is probably attributed to the morphological effect.

3.3.2. Flory Interaction Parameter

The Flory interaction parameter ($\chi_{1,2}$) and the interaction energy density (B), which characterized the interactional dynamics between the two different macromolecules in the blend, were determined by the Nishi–Wang equation (Equation (2)) [40] based on the Flory–Huggins theory. According to Qui et al. [34], regarding the crystalline polymer (1)/crystalline polymer blend (2), as in our case, T_c applied in the equation of Hoffman–Weeks to determine T_m^o of 1 must be higher than that applied to determine T_m^o of 2. Under this condition, 1 acts as a crystalline polymer, whereas 2 is an amorphous polymer. For polymers with high molecular masses, the Nishi–Wang equation can be written as follows:

$$\frac{1}{T_m^o(\text{blend})} = \frac{RV_2\chi_{1,2}}{\Delta H^o V_1} \varphi_1^2 + \frac{1}{T_m^o(\text{pure})} \quad (2)$$

where, $T_m^o(\text{pure})$ and $T_m^o(\text{blend})$ are the equilibrium melting temperatures of the pure crystallizable component possessing a high melting point and the blend, ΔH^o is the enthalpy of

melting 100% of the 1 repeated units, and V_i and ϕ_1 are the molar volume of the repeated units and the volume fraction of polymer (i) in the blend. Applying the data that were obtained from the literature, $\Delta H_{uE-VAL} = 4.22 \text{ kJ mol}^{-1}$ [41], $V_{uE-VAL} = 37.80 \text{ cm}^3 \text{ mol}^{-1}$ [41], and $V_{uPCL} = 99.65 \text{ cm}^3 \text{ mol}^{-1}$ [42]. The $\chi_{1,2}$ and B values were deduced from the slope and intercept of the linear curve, indicating the inverse of $T_m^{(blend)}$, which was obtained from the data in Table 3, vs. the square of ϕ_{E-VAL} , as displayed in Figure 4.

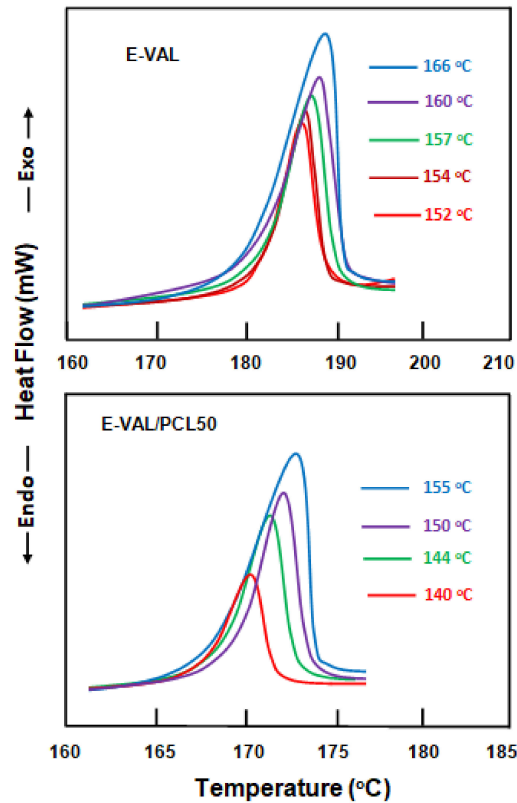


Figure 2. Dynamic DSC thermograms obtained after the isothermal crystallization of E-VAL, and the E-VAL/PCL50 blend at different T_c .

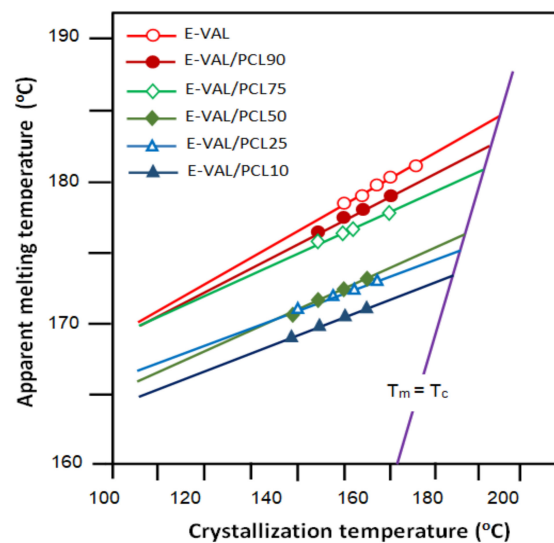


Figure 3. Hoffman–Weeks plots for pure E-VAL and E-VAL/PCL blend with different compositions.

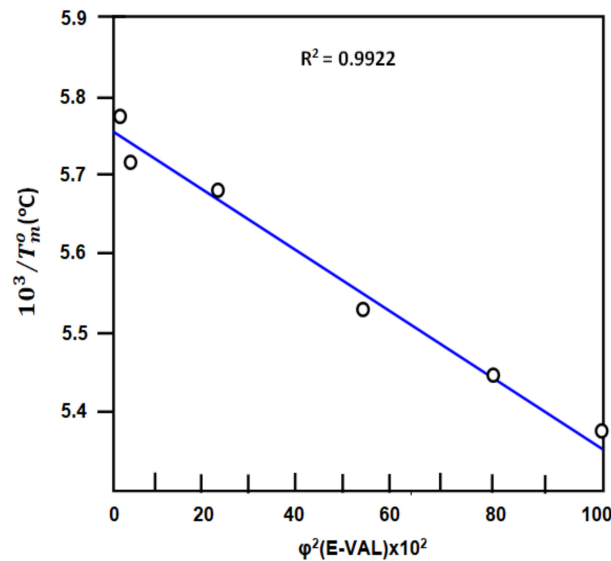


Figure 4. Variation of the inverse of T_m^o vs. the square of $\phi_{\text{E-VAL}}$ in the blend.

The $\chi_{1,2}$ value, which was estimated from the slope of the linear fit, was -0.012 ± 0.002 , and the estimated B value, which was equal to $\chi_{1,2} \text{RTV}_1^{-1}$ [43], was $-1.21 \pm 0.20 \text{ J/cm}^3$ of PCL obtained at 186 °C . According to the Flory–Huggins theory, a negative $\chi_{1,2}$ value indicated that the miscibility of this pair of polymers was caused by specific interactions between the different chains in the blend. These interactions were relatively weak because of the hydrogen bonds in the blend, as previously highlighted by FTIR analysis. The amorphous fraction of the E-VAL/PCL blend is thermodynamically miscible and can form a compatible blend in the melt state.

3.3.3. Crystallization Temperature

In the polymer blend domain, it is well known that the crystallization behavior of each component in a blend depends on its miscibility with the other components, its physicochemical properties, and crystallization conditions. According to Hu et al. [43], the crystallization of one component in a blend affects the morphology, crystallization, and mechanical properties of the second component. Figure 5 shows the DSC cooling thermograms of pure semicrystalline E-VAL, PCL, and their blends, obtained in the non-isothermal crystallization process at a cooling rate of 20 °C min^{-1} . Expectedly, these thermal curves exhibited two distinct exothermic peaks for each blend. The peaks were attributed to the crystallization temperature of each polymer in the blend, and Table 4 illustrates their values.

The percentage crystallization of each component in the blend was calculated from Equation (3) [44], and Table 4 lists the results.

$$X(\%) = \frac{\Delta H_m - \Delta H_c}{w \times \Delta H_m^o} \times 100, \quad (3)$$

where ΔH_m and ΔH_m^o are the heat of fusion of the semicrystalline polymer in the blend and that of the pure polymer with 100% crystallinity for E-VAL = 157.83 J g^{-1} [44] and PCL = 135.5 J g^{-1} [45], respectively. ΔH_c and w are the heat of crystallization of the semicrystalline polymer and its weight fraction, respectively.

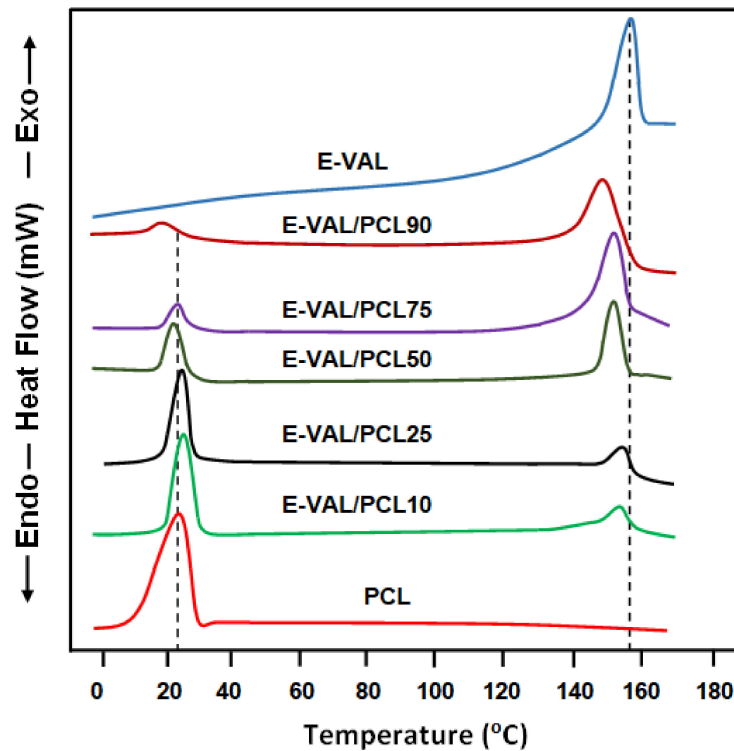


Figure 5. DSC cooling thermograms of E-VAL/PCL blends and their components.

Table 4. Temperatures and heats of crystallization of E-VAL/PCL blends and their pure components.

System E-VAL/PCL	PE-VAL			PCL		
	T_c (°C)	ΔH_c (J/g)	X_c (%)	T_c (°C)	ΔH_c (J/g)	X_c (%)
E-VAL	157	−54.18	48.20	-	-	-
E-VAL/PCL90	148	−52.11	42.56	18	−5.76	5.22
E-VAL/PCL75	152	−26.32	34.22	23	−10.08	9.65
E-VAL/PCL50	152	−23.09	28.34	22	−17.27	15.02
E-VAL/PCL25	154	−12.50	23.08	24	−25.91	22.10
E-VAL/PCL10	154	−10.21	15.21	25	−39.59	33.50
PCL	-	-	-	26	−65.54	52.30

The normalized crystallinity of PCL in the blend decreased dramatically from 52.30% to 5.22% and was accompanied by an increase in the crystallinity of E-VAL from 15.21% to 48.20% when the E-VAL content passed from 0 to 100 wt%. The presence of E-VAL with PCL in the blend severely reduced their respective crystallinities.

The DSC cooling thermograms of the blends and their pure components were obtained at cooling rates of 5, 10, 15, and 20 °C min^{−1}. Figure 6 shows the comparison of the thermal curves of E-VAL/PCL50 and E-VAL/PCL75, employed as examples, with those of the pure components. As shown in these curve profiles, the crystallization temperature shifted to the right as the cooling rate decreased. A significant depression was also observed in the crystallization heat with decreasing cooling rate. This was also observed by different researchers utilizing different pairs of polymers [46,47].

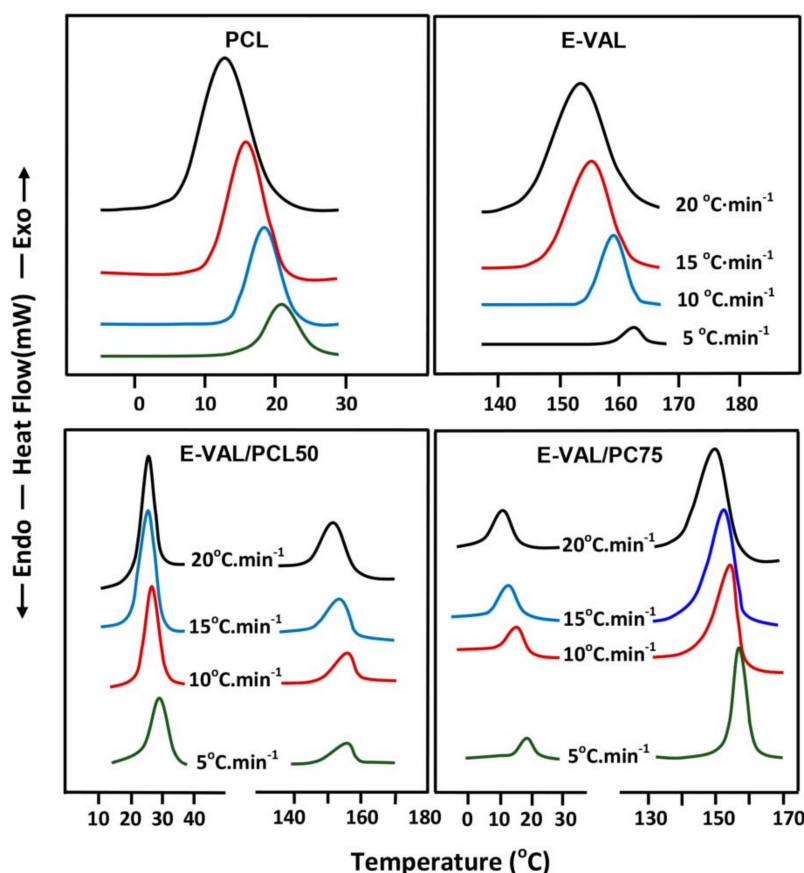


Figure 6. Variation of the crystallization temperatures of E-VAL, PCL, and E-VAL/PCL blends containing 25 and 75 wt% PCL vs. the cooling rates.

3.4. XRD Analysis

Figure 7 shows the XRD patterns of the E-VAL/PCL blends and their components. The spectra of the blend with different compositions revealed the combination of the diffraction peaks of each localized pure polymer of E-VAL at $2\theta = 20$ and 29.22° , which were assigned to the (110) and (200) reflection planes, respectively, and to the orthorhombic forms of polyethylene [48] and PCL at 16° , 22° , and 24° , which are assigned to the reflection planes of (110), (111), and (200), respectively [49,50]. The absence of new diffraction peaks in the spectra of the blend indicated the non-formation of a new crystalline structure. Put differently, E-VAL and PCL preserved their distinct initial crystalline structures in the blend, and the miscibility was realized only in their amorphous parts.

3.5. Thermal Stability

Very few reports are available in the literature on the thermal decomposition of E-VAL compared with the abundant reports on their poly(ethylene) (PE) and poly(vinyl alcohol) (PVA) components. Among these reports, only a very limited number of articles discussed the results of the thermal decomposition of this copolymer in detail. Alvarez et al. [51] suggested that the products, which were obtained from the first step between 387°C and 407°C , involved the decomposition of a greater part of the vinyl alcohol units, whereas the second step involved the decomposition of the ethylene units at higher temperatures. According to different authors [52], the thermal decomposition of PVA principally leads to the production of water and carbon dioxide because of the elimination reactions. Conversely, Kumar and Sing [53] investigated the thermal degradation of PE in which the main products were different volatile saturated and unsaturated hydrocarbons. Thus far, there are no published articles on the fragments, which are obtained from combining ethylenic alcohol and vinyl alcohol units in a copolymer. Regarding the thermal decomposition of

PCL, Persenaire et al. [54] and Vogel et al. [55] concluded that the decomposition process proceeded in two steps: the first caused a statistical rupture of the PCL chains to produce H_2O , CO_2 , and hexanoic acid, and the second is characterized by an unzipping depolymerization process, which causes the regeneration of a monomer (ϵ -caprolactone). Although very few authors have discussed this subject, our contribution in this section is to present a more precise idea of the fragments that are obtained from the thermal decompositions of the two polymers and their blends. To achieve this goal, two complementary techniques were applied to elucidate the decomposition process of the blend and its components. The first, which was non-isothermal, was performed by TGA to elucidate the thermal stability of these materials and their different stages of decomposition, and the second, which was isothermal, was conducted by DART-ToF-MS to determine the main fragments that were obtained from the decomposition, which could not be analyzed by TGA.

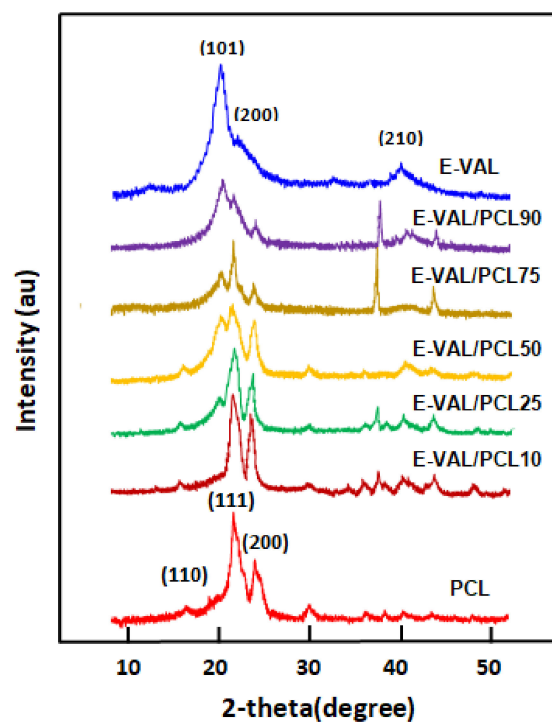


Figure 7. X-ray diffractograms of E-VAL, PCL, and their blends with different compositions.

3.5.1. TGA Analysis

The thermal decompositions of the E-VAL/PCL blends and their pure components were conducted by TGA/derivative-TGA (DTGA) analysis, and Figure 8 lists the obtained thermal curves. The thermograms of pure E-VAL revealed the ultimate decomposition step, which started at 360 °C, whereas that of pure PCL revealed two decomposition steps in which the first and second were at 310 °C (weight loss 9.09 wt%) and 435 °C (weight loss 90.91 wt%), respectively. As shown in the profiles of the E-VAL/PLC curves, similar trends to those of pure E-VAL were observed. These thermograms exhibited only one decomposition temperature, except that containing 90 wt% E-VAL (E-VAL/PCL90) exhibited three distinct decomposition temperatures at 310°C (weight loss 9.09 wt%), 435°C (weight loss 27 wt%), and 445 °C (weight loss 63.91 wt%). Enhanced thermal stability was generally observed in PCL when E-VAL was incorporated in the copolymer matrix. Indeed, the decomposition temperature of the blend shifted positively from 320 °C to 350 °C according to the E-VAL content of the blend. For clarification, just observe the effect of adding 10 wt% E-VAL, which contributed to an increase in the stability of PCL by 20 °C. By contrast, it was observed that the addition of only 10 wt% PCL to the blend dramatically reduced the decomposition temperature of E-VAL from 360 °C to 250 °C. This

finding also revealed the molecular interactions between E-VAL and PCL in the blend. A similar conclusion was also reported on the thermal decomposition of the acetylated starch/poly(ethylene-co-vinyl alcohol) by Jiang et al. [56] These authors also revealed the second decomposition of all the samples at 425 °C. Therein, more than 80 wt% of the polymers or blends were volatilized in form of small molecules, such as carbon dioxide, ethylene, aldehyde, and ketone.

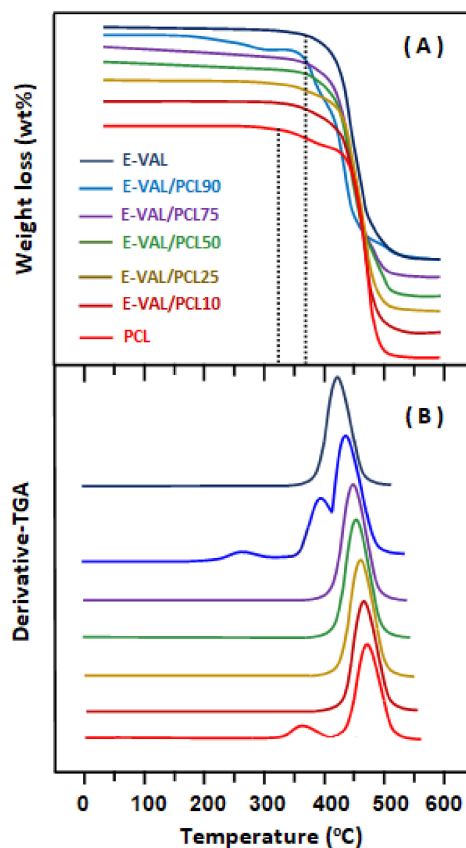


Figure 8. (A) TGA and (B) DTGA thermograms of pure E-VAL, pure PCL, and E-VAL/PCL with different E-VAL contents.

3.5.2. DART-ToF-MS Analysis

Figure 9 lists the spectra of the isothermal decompositions of the blends and their pure components, as obtained by DART-ToF-MS at 350 °C. The E-VAL spectrum revealed a series of signals, which accrued from the fragmentation of this copolymer, and Table 5 presents their main formulas. These compounds were produced by a radical mechanism, which involved chain scission, followed by the random transposition of the different groups that were detached and recombined afterward. As shown in these data, the absence of monomers indicated the absence of depolymerization reaction. However, the intense signal, which was observed at 223.09 m/z , was probably attributed to the isomers of the ferulic acid ethyl ester ($C_{12}H_{15}O_4$) containing 6° of unsaturation. The less-intense signals at 195.12, 235.20, and 344.23 m/z were probably assigned to the tetramer of the vinyl alcohol ($C_8H_{18}O_5$), the isomers of (2*E*,4*S*,6*E*,11*R*)-4,11-dihydroxy-2,6-dodecadienoic acid ($C_{12}H_{20}O_4$), and the isomers of $C_{20}H_{34}O_7$ containing four degrees of unsaturation, respectively. Conversely, the isothermal decomposition of pure PCL generated five main compounds and a small amount of the monomer, as presented in Table 6. However, the spectrum of the E-VAL/PCL50 blend was revealed by its data in Table 7. In addition to the signals that were attributed to the two pure components, other signals indicating the presence of new fragments were obtained from a possible transposition and combination of the radical groups from one chain to a neighboring chain of a different nature. This could

also be considered as proof of the miscibility of this system since a radical transposition reaction can only proceed when the two components are close, as in a miscible blend.

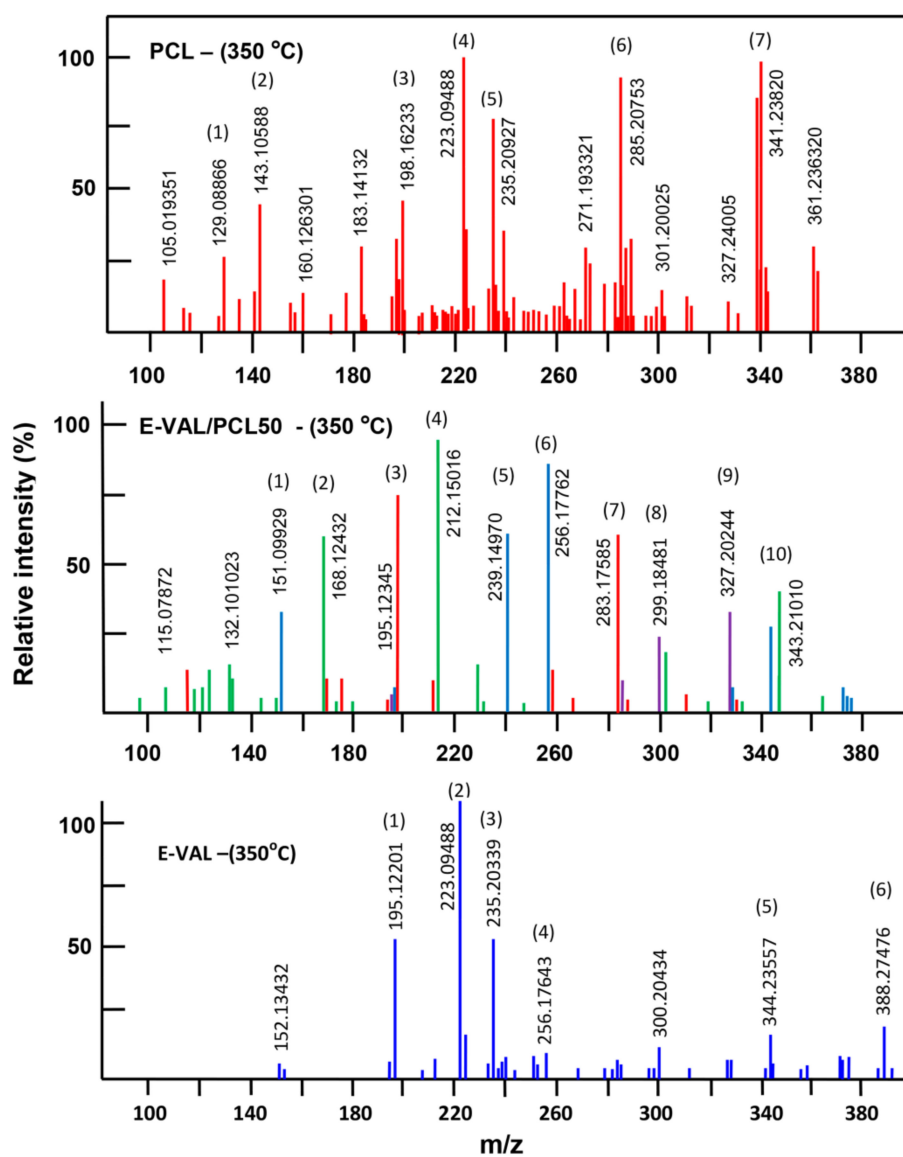


Figure 9. The spectra of the isothermal decompositions of the blends and their pure components, as obtained by DART-ToF-MS at 350 °C.

Table 5. Principal fragments obtained by the isothermic decomposition of pure E-VAL.

N°	Experimental Mass	Calculated Mass	Formula
1	195.12201	195.12183	$C_8H_{18}O_5$
2	223.09488	223.09703	$C_{12}H_{15}O_4$
3	235.20339	235.20619	$C_{16}H_{27}O$
4	256.17643	256.17869	$C_{13}H_{24}N_2O_3$
5	344.23557	344.23112	$C_{17}H_{32}N_2O_5$
6	388.25476	388.25734	$C_{19}H_{36}N_2O_6$

Table 6. Principal fragments obtained by the isothermic decomposition of PCL.

Nº	Experimental Mass	Calculated Mass	Formula
1	129.08866	129.09155	C ₇ H ₁₂ O ₂
2	143.10588	143.10720	C ₈ H ₁₄ O ₂
3	198.16233	198.16198	C ₁₂ H ₂₁ O ₂
4	223.09488	223.09703	C ₁₂ H ₁₅ O ₄
5	235.20927	235.20619	C ₁₆ H ₂₇ O
6	285.20753	285.20658	C ₁₆ H ₂₉ O ₄
7	341.23820	341.23280	C ₁₉ H ₃₃ O ₅

Table 7. Principal fragments obtained by the isothermal decomposition of E-VAL/PCL50.

Nº	Experimental Mass	Calculated Mass	Formula
1	115.07872	115.07590	C ₆ H ₁₁ O ₂ (monomer)
2	151.09929	151.09971	C ₉ H ₁₃ NO
3	195.12345	195.12325	C ₈ H ₁₉ O ₅
4	212.15016	212.14979	C ₇ H ₁₆ N ₈
5	239.14970	239.14946	C ₁₀ H ₂₃ O ₆
6	256.17762	256.17735	C ₁₁ H ₂₂ N ₅ O ₂
7	283.17585	283.17568	C ₁₂ H ₂₇ O ₇
8	299.18481	299.18585	C ₁₆ H ₂₇ O ₅
9	327.20244	327.20189	C ₁₄ H ₃₁ O ₈
10	343.21010	343.21206	C ₁₈ H ₃₁ O ₆

3.6. Non-Isothermal Crystallization Kinetics

3.6.1. The Relative Degree of Crystallization

The relative degree of crystallinity (X_T), as a function of T_c , is expressed by Equation (4) [57]:

$$X_T = \frac{\int_{T_0}^T \left(\frac{dH}{dt} \right) dt}{\int_{T_0}^{T_\infty} \left(\frac{dH}{dt} \right) dt} \quad (4)$$

where T_0 and T_∞ are the starting and ending T_c that were obtained at the starting and ending inflections of the crystallization peak, respectively, and H is the instantaneous enthalpy of the crystallization process. After substituting the areas of the DSC thermograms, Equation (5) would be expressed as follows:

$$X_T = \frac{A_T}{A_\infty} \quad (5)$$

where A_T and A_∞ are the areas under the DSC curves from $T = T_0$ to $T = T$ and the total area under the crystallization curve, respectively. X_T could be determined by employing this equation at a specific temperature. During non-isothermal crystallization, the variation in the crystallization time with the crystallization temperature follows Equation (6):

$$t = \frac{(T_0 - T)}{\beta} \quad (6)$$

where T and β are the temperature at a crystallization time, t , and the cooling rate, respectively. The integration of the exothermic peaks during the non-isothermal scans afforded X_T , as a function of the temperature, as shown in Figure 10 for E-VAL, PCL, and the E-VAL/PCL50 blend.

Because of the effect of retardation on crystallization, all the curves exhibited an approximately sigmoid pattern. The typical plots of X_t vs. time for E-VAL, PCL, and their blends with equal composition were traced by combining Equations (4)–(6), as shown in Figure 11.

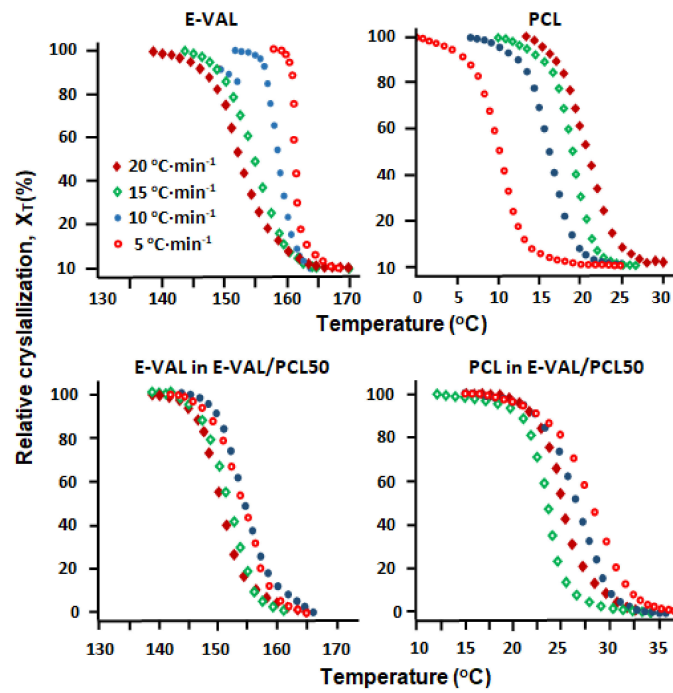


Figure 10. Variation in X_T of E-VAL, PCL, E-VAL in E-VAL/PCL50, and PCL in E-VAL/PLC50 with the temperature at different crystallization rates.

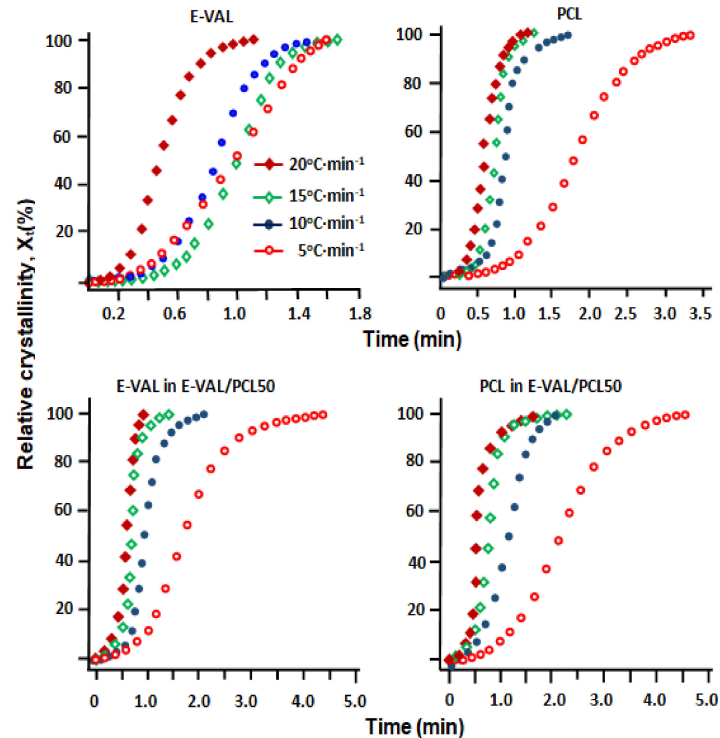


Figure 11. Variation of X_T of E-VAL, PCL, E-VAL in E-VAL/PCL50, and PCL in E-VAL/PLC50 with time at different crystallization rates.

Similar to the plots of X_T vs. temperature, all the curves exhibited largely sigmoid patterns, and the slopes of these curves at each point corresponded to the rate of crystallization. As observed from these sigmoid profiles, the rate of crystallization was almost

constant between 20% and 80% of X_T . At the later stage, the curves appeared flat because of spherulite impingement [58].

3.6.2. Half-Time of the Crystallization

The half times ($t_{1/2}$) for completing the crystallization for the pure polymer, pure copolymer, and their blends, as deduced from the curves, indicate the variation in X_t vs. time at 50% X_T , and Table 8 summarizes the results obtained. As shown in these curve profiles, $t_{1/2}$ of pure PCL and E-VAL generally decreased slightly as the cooling rate increased, passing from 1.8 to 0.6 min for the first polymer and 1.0 to 0.5 min for the second as the cooling rate passed from 5 to 20 °C min⁻¹. Similar values and trends were also observed by Yung et al. [59] and Zhu et al. [60]. The variation of $t_{1/2}$ vs. the E-VAL content of the E-VAL/PCL system attained a minimum of 1.6 min at 5 °C min⁻¹ for the blend containing 90 wt% E-VAL. In the same direction contrast to the pure E-VAL, the $t_{1/2}$ values decreased with increasing cooling rate. This is because, at a relatively high PCL content, the molecules of the E-VAL clusters can restrict the motion of the PCL molecular chains, although they cannot act as a heterogeneous nucleating agent in the non-isothermal crystallization process to accelerate crystallization. However, with an increased PCL content, the molecular chains of these polymer clusters could act as a barrier to restrict the thermal motion of the molecular chains of E-VAL, thereby retarding the formation of crystals. Therefore, the addition of a large amount of PCL can delay the overall crystallization process.

Table 8. Temperatures and $t_{1/2}$ of the crystallization of E-VAL and the E-VAL/PCL blends obtained by the non-isothermal crystallization kinetics.

Samples	β (°C.min ⁻¹)	T_c (°C)		$t_{1/2}$ (min)	
		PCL	E-VAL	PCL	E-VAL
PCL	5	21	-	1.8	-
	10	19	-	0.8	-
	15	16	-	0.7	-
	20	10	-	0.6	-
E-VAL/PCL10	5	30	157	1.8	2.4
	10	27	156	0.8	1.2
	15	26	153	0.5	0.8
	20	25	152	0.5	0.5
E-VAL/PCL25	5	30	156	2.0	2.2
	10	28	154	1.0	1.1
	15	26	152	0.7	1.0
	20	25	151	0.6	0.8
E-VAL/PCL50	5	30	154	2.2	1.7
	10	28	155	1.2	0.9
	15	27	153	0.8	0.7
	20	25	152	0.5	0.6
E-VAL/PCL75	5	19	157	1.2	2.6
	10	16	154	0.8	1.9
	15	13	152	0.6	1.4
	20	11	150	0.5	1.2
E-VAL/PCL90	5	-	161	1.0	1.6
	10	-	159	0.7	1.3
	15	-	158	0.6	1.1
	20	-	157	0.5	0.8
E-VAL	5	-	155	-	1.0
	10	-	152	-	0.9
	15	-	150	-	1.0
	20	-	148	-	0.5

3.6.3. Ozawa Parameters

The Ozawa relationship (Equation (7)) [31], which is an extension of the Avrami equation (Equation (8)) [61], was adopted to investigate the non-isothermal crystallization of the pure polymer and its blend at various cooling rates.

$$1 - X_T = \exp\left(-\frac{k_T}{\beta^m}\right) \quad (7)$$

$$1 - X_t = \exp(-kt^n) \quad (8)$$

The Avrami equation, which is originally applied to isothermal crystallization, could also be applied to non-isothermal crystallization by assuming that the specimen was cooled at a constant cooling rate. Accordingly, X_t and X_T represent the relative degrees of crystallinity at a time (t) and temperature (T), respectively; k and k_T are the rate constant of the crystallization kinetics and cooling function of the non-isothermal crystallization at temperature (T), respectively; β is the cooling rate; and n and m are the isothermal Avrami and Ozawa exponents based on the dimensions of the crystal growth and nucleation mechanism, respectively. Thus, Equation (9) can be linearized as follows:

$$\ln[-\ln(1 - X_T)] = \ln k_T - m \ln \beta \quad (9)$$

As shown in the plots of $\ln[-\ln(1 - X_t)]$ vs. $\ln(\beta)$ for E-VAL and the E-VAL/PCL50 system, which were adopted as examples (Figure 12), all the specimens containing pure E-VAL and E-VAL/PCL with different PCL contents exhibited straight lines. This revealed that the Ozawa equation (Equation (7)) perfectly described the primary non-isothermal crystallization process. Table 9 summarizes k_T and m , which were deduced from the intercepts and slopes of these curves, respectively. According to these obtained data, the m value of pure E-VAL slightly increased from 1.97 to 2.33, whereas that of pure PCL passed from 1.73 to 2.67 with the crystallization temperature.

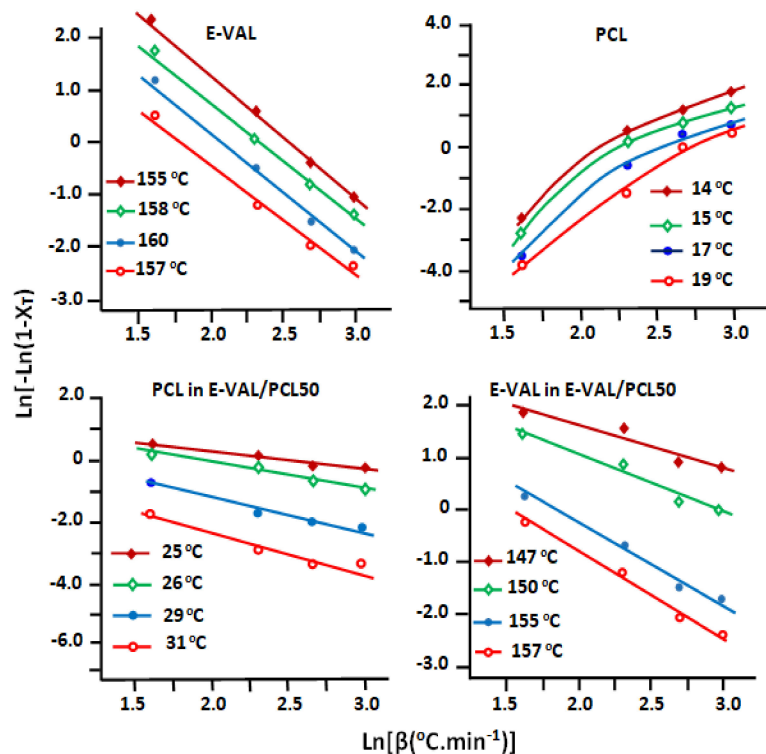


Figure 12. Ozawa plots indicating the variation of $\ln[-\ln(1 - X_t)]$ vs. $\ln(\beta)$ for pure E-VAL and the E-VAL/PCL blend containing 75 wt% E-VAL.

Table 9. Ozawa parameters representing the non-isothermal crystallization kinetics of pure E-VAL, PCL, PCL in E-VAL/PCL, and E-VAL in E-VAL/PCL.

Sample	T_c (°C)		m		k_T	
	PCL	E-VAL	PCL	E-VAL	PCL	E-VAL
PCL	14	-	1.73	-	3.7×10^{-3}	-
	15	-	1.60	-	4.4×10^{-3}	-
	17	-	1.87	-	7.4×10^{-3}	-
	19	-	2.67	-	1.9×10^{-3}	-
E-VAL/PCL10	16	145	1.45	0.72	1.5×10^{-3}	18.91
	18	150	1.46	0.74	1.4×10^{-3}	13.46
	20	155	1.72	0.75	1.1×10^{-3}	10.17
	22	160	2.39	0.82	1.0×10^{-3}	5.99
E-VAL/PCL25	19	146	1.17	0.96	7.1×10^{-2}	9.47
	21	151	1.32	1.21	1.1×10^{-2}	6.56
	23	155	1.53	1.26	1.9×10^{-3}	4.64
	25	158	2.10	1.31	6.6×10^{-4}	3.05
E-VAL/PCL50	25	147	0.60	1.21	1.4×10^{-1}	0.17
	27	153	1.0	1.23	2.0×10^{-2}	0.14
	28	155	1.2	1.62	2.7×10^{-3}	0.04
	31	157	1.5	1.80	2.8×10^{-4}	0.06
E-VAL/PCL75	23	155	0.54	0.87	4.6×10^{-2}	0.37
	25	157	0.83	1.10	7.1×10^{-3}	0.19
	27	160	0.94	1.20	3.4×10^{-3}	0.10
	30	162	1.21	1.52	3.2×10^{-3}	0.04
E-VAL	-	148	-	1.97	-	1.8×10^{-2}
	-	150	-	2.12	-	94.63
	-	152	-	2.21	-	86.48
	-	155	-	2.33	-	84.77

These results are similar to those reported in the literature: 1.93–2.27 for E-VAL [47] and 2.1–2.5 for PCL [62]. Conversely, the values of m for E-VAL and PCL in the E-VAL/PCL blend increased with the temperature, indicating that the incorporation of E-VAL into the PCL matrix greatly influenced the growth of the crystals. A slight increase in m , which was observed as the temperature increased, revealed a dramatic change in the crystallization mechanism. This was probably because of an increase in the viscosity of the blend, which was caused by the weak rupture of the hydroxyl–hydroxyl groups of E-VAL to favor the relatively high interactions between the hydroxyl and carbonyl groups of E-VAL and PCL, respectively, thereby supporting the miscibility behavior of this pair of polymers. From these data, it was generally revealed that the m value of E-VAL was dramatically reduced by the addition of PCL. For example, at 155 °C, m passed from 2.33 to 0.75 when the PCL content of the blend varied from 0 to 90 wt%. Similar results were also obtained for the m values of PCL, although they were less-noticeable with increasing E-co-VAL contents. Moreover, an increase in the m value is generally attributed to the change from sporadic to instantaneous nucleation [63]. According to typical polymer crystallization reports, an m value of ~ 2 indicated that the crystal growth occurred in the nuclei and was sporadic and spherical. Heterogeneous nucleation has been attributed to the fractional m values that were obtained during polymer crystallization [64]. The k_T value, which is related to the overall crystallization rate, decreased as the temperature decreased, indicating that for E-VAL and the E-VAL/PCL blend with these compositions, the crystallization rate increased as the temperature decreased, notably in the case of pure E-VAL in 3.2.2.

3.6.4. Crystallization Activation Energy (E_c)

E_c , which is associated with the overall crystallization process, was evaluated from the rates of crystallization and temperature that were recorded at the top of the crystallization peak of the polymer employing the Kissinger equation (Equation (10)) as follows [65]:

$$E_c = \frac{d[\ln(\beta/T_c^2)]}{d(1/T_c)} R \quad (10)$$

where R and T_c are the gas constant and peak crystallization temperature, respectively. E_c was obtained from the slope of $RLn\left(\frac{\beta}{T_c^2}\right)$ vs. $1/T$, which was plotted, as shown in Figure 13. As shown by the curve profiles of the pure polymer, copolymer, and blends, straight lines were obtained, and Table 10 summarizes the obtained E_c values. These data revealed negative values for E_c , indicating that the crystallization process was accompanied by the release of heat. These data revealed that the E_c values of pure PCL and E-VAL were -120 and -145 kJ mol^{-1} , respectively, which are slightly inferior to those obtained by Wei et al. (-145 kJ mol^{-1}) [66] and Zhua et al. (-239 kJ mol^{-1}) [60] for PCL and E-VAL, respectively. These values were severely affected by the incorporation of one of the components into the other. Indeed, E_c of PCL in the blend passed by a maximum of 291 kJ mol^{-1} with an equal ratio of E-VAL/PCL, whereas that of E-VAL decreased continuously. For all the cases and at any composition, the E_c values of the blends were superior to those of their pure constituents. According to Yang et al. [67], a more negative value of the activation energy means that more heat would be released for the crystallization. In this case, this indicates that it is more challenging to perform the crystallization process of each component in the blend than in their respective pure states.

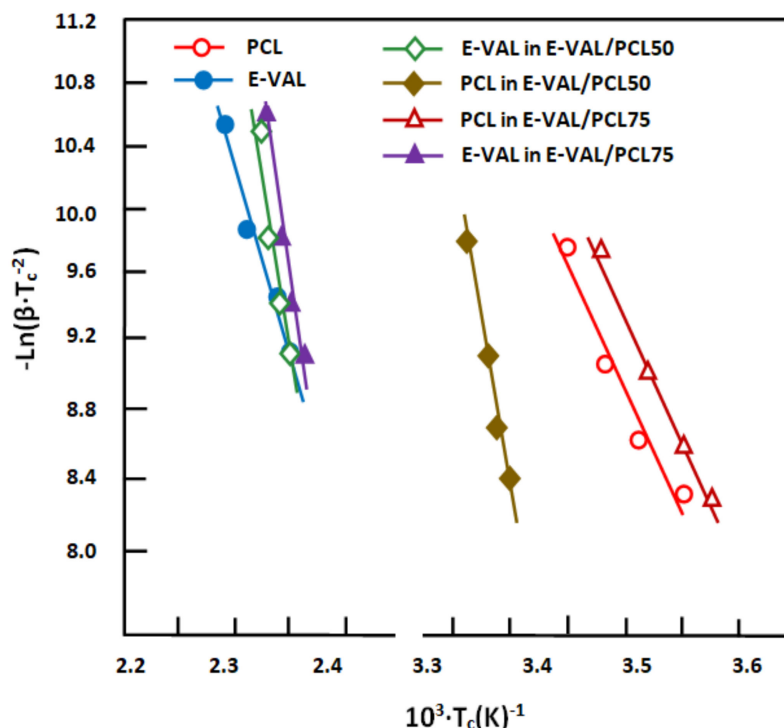


Figure 13. Variation of $\ln(\beta/T_c^2)$ vs. the inverse of the temperature of pure E-VAL and E-VAL/PCL containing 75 and 10 wt% E-VAL.

Table 10. Activation energies of the crystallization of pure E-VAL, PCL, PCL in E-VAL/PCL, and E-VAL in E-VAL/PCL.

Sample	E_a (kJ.mol ⁻¹)	
	PCL	E-VAL
PCL	−120.0	-
E-VAL/PCL10	−241.1	−295.2
E-VAL/PCL25	−262.7	−275.2
E-VAL/PCL50	−291.0	−266.2
E-VAL/PCL75	−144.7	−206.4
E-VAL/PCL90	−132.3	−194.2
E-VAL	-	−180.8

4. Conclusions

Conclusively, the objective of this investigation, i.e., the miscibility of the E-VAL/PCL blend in the investigated composition range, was achieved by obtaining a negative value (−1.21) for the Flory interaction parameter between its components through the Nishi–Wang equation. Generally, the thermal stability of the obtained material, which was analyzed by TGA, revealed a drastic increase in the thermal stability of PCL with increasing E-VAL contents of the blend. For example, the incorporation of only 10 wt% E-VAL increased the thermal stability of PCL by 20 °C. Conversely, the addition of only 10 wt% PCL to the blend dramatically decreased the decomposition temperature of E-VAL. The isothermal decompositions of the pure components and their blends, which were analyzed by DART-ToF-MS at 350 °C, revealed the non-generation of monomers for E-VAL. However, a series of the isomers of ferulic acid ethyl esters, the tetramers of vinyl alcohol (C₈H₁₈O₅), the isomers of (2*E*,4*S*,6*E*,11*R*)-4,11-dihydroxy-2,6-dodecadienoic acid (C₁₂H₂₀O₄), and the isomers of C₂₀H₃₄O₇ were observed. Conversely, pure PCL generated five main compounds, as well as a few monomers. In addition to the fragments of the two components, the thermal fragmentation of E-VAL/PCL at the same temperature generated new compounds probably through the transposition and recombination of the radical groups from one chain to a neighboring chain of different natures. Furthermore, this finding can be employed as supplementary proof of the miscibility of this polymer system. The non-isothermal crystallization kinetics, which was obtained for the E-VAL/PCL blends and their components, revealed that the Ozawa model well-described their crystallization behaviors. It was observed from this investigation that the Ozawa exponent decreased as one of the two components in the blend increased. The Kissinger equation was adapted to determine the activation energies for the investigated blends and their pure components. Indeed, the Kissinger plots were obtained, and their slopes exhibited negative values of E_c , which indicated that the crystallization process was exothermic and that the activation energies were severely affected by the incorporation of one of the components into the blend.

Author Contributions: Data curation, A.A.A., H.A., W.S.S., A.-B.A.-O., A.Y.B.H.A. and A.A.A.-O.; Formal analysis, H.A., W.S.S. and A.Y.B.H.A.; Funding acquisition, A.A.A.; Investigation, A.A.A.-O.; Methodology, A.A.A., H.A. and T.A.; Project administration, T.A.; Resources, A.-B.A.-O.; Software, W.S.S.; Supervision, T.A.; Validation, H.A. and W.S.S.; Visualization, W.S.S. and A.-B.A.-O.; Writing—original draft, T.A.; Writing—review & editing, T.A. All authors have read and agreed to the published version of the manuscript.

Funding: The authors extend their appreciation to the Deanship of Scientific Research at King Saud University for funding this work through Research Group No. RGP-VPP-025.

Informed Consent Statement: Not applicable.

Data Availability Statement: All the data supporting the findings of this study are available within the article.

Conflicts of Interest: The authors declare no conflict of interest.

References

1. Feng, C.; Li, Y.; Yang, D.; Hu, J.; Zhang, X.; Huang, X. Well-defined graft copolymers: From controlled synthesis to multipurpose applications. *Chem. Soc. Rev.* **2011**, *40*, 1282–1295. [[CrossRef](#)]
2. Nomura, N.; Akita, A.; Ishii, R.; Mizuno, M. Random Copolymerization of ϵ -Caprolactone with Lactide Using a Homosalen-Al Complex. *J. Am. Chem. Soc.* **2010**, *132*, 1750–1751. [[CrossRef](#)] [[PubMed](#)]
3. McGrath, J.E.; McGrath, J.E. *Block Copolymers: Overview and Critical Survey*; Academic Press: Cambridge, MA, USA, 1977.
4. Ceresa, R.J. Block and graft copolymers. *AIChE J.* **1962**, *9*, 715–718.
5. van Eerdenbrugh, B.; Taylor, L.S. Molecular weight effects on the miscibility behavior of dextran and maltodextrin with poly(vinylpyrrolidone). *Pharm. Res.* **2012**, *29*, 2754–2765. [[CrossRef](#)]
6. Utracki, L. Economics of polymer blends. *Polym. Eng. Sci.* **1982**, *22*, 1166–1175. [[CrossRef](#)]
7. Marco, C.; Fatou, J.; Gomez, M.; Tanaka, H.; Tonelli, A. Molecular weight effect on the miscibility of poly(ethylene oxide) and isotactic poly(methyl methacrylate) in their blends. *Macromolecules* **1990**, *23*, 2183–2188. [[CrossRef](#)]
8. Lam, C.X.; Savalani, M.M.; Teoh, S.-H.; Hutmacher, D.W. Dynamics of in vitro polymer degradation of polycaprolactone-based scaffolds: Accelerated versus simulated physiological conditions. *Biomed. Mater.* **2008**, *3*, 034108. [[CrossRef](#)] [[PubMed](#)]
9. Albertsson, A.-C.; Varma, I.K. Recent developments in ring opening polymerization of lactones for biomedical applications. *Biomacromolecules* **2003**, *4*, 1466–1486. [[CrossRef](#)]
10. Augustine, R.; Kalarikkal, N.; Thomas, S. Advancement of wound care from grafts to bioengineered smart skin substitutes. *Prog. Biomater.* **2014**, *3*, 103–113. [[CrossRef](#)] [[PubMed](#)]
11. Holländer, J.; Genina, N.; Jukarainen, H.; Khajeheian, M.; Rosling, A.; Mäkilä, E.; Sandler, N. Three-dimensional printed PCL-based implantable prototypes of medical devices for controlled drug delivery. *J. Pharm. Sci.* **2016**, *105*, 2665–2676. [[CrossRef](#)] [[PubMed](#)]
12. Boia, R.; Dias, P.A.; Martins, J.M.; Galindo-Romero, C.; Aires, I.D.; Vidal-Sanz, M.; Agudo-Barriuso, M.; de Sousa, H.C.; Ambrósio, A.F.; Braga, M.E. Porous poly(ϵ -caprolactone) implants: A novel strategy for efficient intraocular drug delivery. *J. Control. Release* **2019**, *316*, 331–348. [[CrossRef](#)] [[PubMed](#)]
13. Silva-Cunha, A.; Fialho, S.L.; Naud, M.-C.; Behar-Cohen, F. Poly- ϵ -caprolactone intravitreal devices: An in vivo study. *Investig. Ophthalmol. Vis. Sci.* **2009**, *50*, 2312–2318. [[CrossRef](#)]
14. Stewart, S.A.; Domínguez-Robles, J.; McIlorum, V.J.; Gonzalez, Z.; Utomo, E.; Mancuso, E.; Lamprou, D.A.; Donnelly, R.F.; Larranñeta, E. Poly(caprolactone)-Based Coatings on 3D-Printed Biodegradable Implants: A Novel Strategy to Prolong Delivery of Hydrophilic Drugs. *Mol. Pharm.* **2020**, *17*, 3487–3500. [[CrossRef](#)]
15. Luciani, A.; Coccoli, V.; Orsi, S.; Ambrosio, L.; Netti, P.A. PCL microspheres based functional scaffolds by bottom-up approach with predefined microstructural properties and release profiles. *Biomaterials* **2008**, *29*, 4800–4807. [[CrossRef](#)]
16. Lee, K.; Kim, H.; Khil, M.; Ra, Y.; Lee, D. Characterization of nano-structured poly(ϵ -caprolactone) nonwoven mats via electrospinning. *Polymer* **2003**, *44*, 1287–1294. [[CrossRef](#)]
17. de Biotecnología, G. Poly(vinylalcohol-co-ethylene) biodegradation on semi solid fermentation by *Phanerochaete chrysosporium*. *Acta Farm. Bonaer.* **2004**, *23*, 123–128.
18. Kueng, W.; Silber, E.; Eppenberger, U. Quantification of cells cultured on 96-well plates. *Anal. Biochem.* **1989**, *182*, 16–19. [[CrossRef](#)]
19. Matsumura, K.; Hyon, S.H.; Nakajima, N.; Peng, C.; Tsutsumi, S. Surface modification of poly(ethylene-co-vinyl alcohol)(EVA). Part I. Introduction of carboxyl groups and immobilization of collagen. *J. Biomed. Mater. Res.* **2000**, *50*, 512–517. [[CrossRef](#)]
20. Ino, J.M.; Chevallier, P.; Letourneur, D.; Mantovani, D.; Le Visage, C. Plasma functionalization of poly(vinyl alcohol) hydrogel for cell adhesion enhancement. *Biomater* **2013**, *3*, e25414. [[CrossRef](#)] [[PubMed](#)]
21. Mandelkern, L. *Crystallization of Polymers: Volume 2, Kinetics and Mechanisms*; Cambridge University Press: Cambridge, UK, 2004.
22. Bartczak, Z. Deformation of semicrystalline polymers—The contribution of crystalline and amorphous phases. *Polimery* **2017**, *62*, 787–799. [[CrossRef](#)]
23. Luo, D.-J.; Shao, H.-J.; Wei, F.-J.; Zhang, K.-Z.; Cui, Z.-Y.; Yu, J.; Qin, S.-H. Morphology and Isothermal Crystallization Kinetics of Polypropylene/Poly(ethylene-co-vinyl alcohol) Blends. *Int. Polym. Process.* **2019**, *34*, 195–208. [[CrossRef](#)]
24. Peppas, N.A.; Hansen, P.J. Crystallization kinetics of poly(vinyl alcohol). *J. Appl. Polym. Sci.* **1982**, *27*, 4787–4797. [[CrossRef](#)]
25. Pereira, F.M.; Canevarolo, S.V.; Chinelatto, M.A. Isothermal crystallization kinetics of biodegradable poly(lactic acid)/poly(ϵ -caprolactone) blends compatibilized with low-molecular weight block copolymers. *Polym. Eng. Sci.* **2019**, *59*, E161–E169. [[CrossRef](#)]
26. Choi, J.; Chun, S.W.; Kwak, S.Y. Non-Isothermal Crystallization of Hyperbranched Poly(ϵ -caprolactone) s and Their Linear Counterpart. *Macromol. Chem. Phys.* **2006**, *207*, 1166–1173. [[CrossRef](#)]
27. Long, Y.; Shanks, R.A.; Stachurski, Z.H. Kinetics of polymer crystallisation. *Prog. Polym. Sci.* **1995**, *20*, 651–701. [[CrossRef](#)]
28. Tadmor, Z.; Gogos, C.G. *Principles of Polymer Processing*; John Wiley & Sons: Hoboken, NJ, USA, 2013.
29. Jeziorny, A. Parameters characterizing the kinetics of the non-isothermal crystallization of poly(ethylene terephthalate) determined by DSC. *Polymer* **1978**, *19*, 1142–1144. [[CrossRef](#)]
30. Ziabicki, A. Crystallization of polymers in variable external conditions. *Colloid Polym. Sci.* **1996**, *274*, 705–716. [[CrossRef](#)]
31. Ozawa, T. Kinetics of non-isothermal crystallization. *Polymer* **1971**, *12*, 150–158. [[CrossRef](#)]
32. van Berkel, J.G.I. *On the Physical Properties of Poly(Ethylene 2, 5-Furandicarboxylate)*; Université Côte d’Azur: Nice, France, 2018.

33. Alghamdi, A.A.; Alattas, H.; Saeed, W.S.; Al-Odayni, A.-B.; Alrahlah, A.; Aouak, T. Preparation and Characterization of Poly (ethylene-co-vinyl alcohol)/poly (ϵ -caprolactone) Blend for Bioscaffolding Applications. *Int. J. Mol. Sci.* **2020**, *21*, 5881. [[CrossRef](#)]
34. Qiu, Z.; Ikehara, T.; Nishi, T. Miscibility and crystallization in crystalline/crystalline blends of poly (butylene succinate)/poly (ethylene oxide). *Polymer* **2003**, *44*, 2799–2806. [[CrossRef](#)]
35. de Lima, J.A.; Felisberti, M.I. Poly (ethylene-co-vinyl alcohol) and poly (methyl methacrylate) blends: Phase behavior and morphology. *Eur. Polym. J.* **2008**, *44*, 1140–1148. [[CrossRef](#)]
36. Flory, P.J. Thermodynamics of high polymer solutions. *J. Chem. Phys.* **1941**, *9*, 660. [[CrossRef](#)]
37. Huggins, M.L. Solutions of long chain compounds. *J. Chem. Phys.* **1941**, *9*, 440. [[CrossRef](#)]
38. Hoffman, J.D.; Weeks, J.J. X-ray study of isothermal thickening of lamellae in bulk polyethylene at the crystallization temperature. *J. Chem. Phys.* **1965**, *42*, 4301–4302. [[CrossRef](#)]
39. Alvarez, V.A.; Kenny, J.M.; Vázquez, A. Isothermal crystallization of poly (vinyl alcohol-co-ethylene). *J. Appl. Polym. Sci.* **2003**, *89*, 1071–1077. [[CrossRef](#)]
40. Nishi, T.; Wang, T. Melting point depression and kinetic effects of cooling on crystallization in poly (vinylidene fluoride)-poly (methyl methacrylate) mixtures. *Macromolecules* **1975**, *8*, 909–915. [[CrossRef](#)]
41. Lee, J.-C.; Tazawa, H.; Ikehara, T.; Nishi, T. Miscibility and Crystallization Behavior of Poly (butylene succinate) and Poly (vinylidene fluoride) Blends. *Polym. J.* **1998**, *30*, 327–339. [[CrossRef](#)]
42. She, H.; Xiao, X.; Liu, R. Preparation and characterization of polycaprolactone-chitosan composites for tissue engineering applications. *J. Mater. Sci.* **2007**, *42*, 8113–8119. [[CrossRef](#)]
43. Hu, Y.; Sato, H.; Zhang, J.; Noda, I.; Ozaki, Y. Crystallization behavior of poly (l-lactic acid) affected by the addition of a small amount of poly (3-hydroxybutyrate). *Polymer* **2008**, *49*, 4204–4210. [[CrossRef](#)]
44. Oyama, H.T. Super-tough poly (lactic acid) materials: Reactive blending with ethylene copolymer. *Polymer* **2009**, *50*, 747–751. [[CrossRef](#)]
45. Nagata, M.; Yamamoto, Y. Synthesis and characterization of photocrosslinked poly (ϵ -caprolactone) s showing shape-memory properties. *J. Polym. Sci. Part A Polym. Chem.* **2009**, *47*, 2422–2433. [[CrossRef](#)]
46. Hsu, W.P. Reexamination of the miscibility of stereoregular poly (methyl methacrylate) with poly (vinyl phenol). *J. Appl. Polym. Sci.* **2002**, *83*, 1425–1431. [[CrossRef](#)]
47. Alvarez, V.A.; Stefani, P.M.; Vázquez, A. Non-isothermal crystallization of polyvinylalcohol-co-ethylene. *J. Therm. Anal. Calorim.* **2005**, *79*, 187–193. [[CrossRef](#)]
48. Guadagno, L.; Naddeo, C.; Vittoria, V.; Camino, G.; Cagnani, C. Chemical and morphological modifications of irradiated linear low density polyethylene (LLDPE). *Polym. Degrad. Stab.* **2001**, *72*, 175–186. [[CrossRef](#)]
49. Baji, A.; Wong, S.C.; Liu, T.; Li, T.; Srivatsan, T. Morphological and X-ray diffraction studies of crystalline hydroxyapatite-reinforced polycaprolactone. *J. Biomed. Mater. Res. Part B Appl. Biomater.* **2007**, *81*, 343–350. [[CrossRef](#)] [[PubMed](#)]
50. Nanaki, S.G.; Papageorgiou, G.Z.; Bikiaris, D.N. Crystallization of novel poly (ϵ -caprolactone)-block-poly (propylene adipate) copolymers. *J. Therm. Anal. Calorim.* **2012**, *108*, 633–645. [[CrossRef](#)]
51. Alvarez, V.; Ruseckaite, R.; Vázquez, A. Kinetic analysis of thermal degradation in poly (ethylene-vinyl alcohol) copolymers. *J. Appl. Polym. Sci.* **2003**, *90*, 3157–3163. [[CrossRef](#)]
52. Tsuchiya, Y.; Sumi, K. Thermal decomposition products of polyethylene. *J. Polym. Sci. Part A 1 Polym. Chem.* **1968**, *6*, 415–424. [[CrossRef](#)]
53. Holland, B.; Hay, J. The thermal degradation of poly (vinyl alcohol). *Polymer* **2001**, *42*, 6775–6783. [[CrossRef](#)]
54. Persenaire, O.; Alexandre, M.; Degée, P.; Dubois, P. Mechanisms and kinetics of thermal degradation of poly (ϵ -caprolactone). *Biomacromolecules* **2001**, *2*, 288–294. [[CrossRef](#)]
55. Vogel, C.; Siesler, H.W. Thermal Degradation of Poly (ϵ -caprolactone), Poly (L-lactic acid) and their Blends with Poly (3-hydroxybutyrate) Studied by TGA/FT-IR Spectroscopy. *Macromol. Symp.* **2008**, *265*, 183–194. [[CrossRef](#)]
56. Jiang, W.; Qiao, X.; Sun, K. Mechanical and thermal properties of thermoplastic acetylated starch/poly (ethylene-co-vinyl alcohol) blends. *Carbohydr. Polym.* **2006**, *65*, 139–143. [[CrossRef](#)]
57. Guo, Q.; Groeninckx, G. Crystallization kinetics of poly (ϵ -caprolactone) in miscible thermosetting polymer blends of epoxy resin and poly (ϵ -caprolactone). *Polymer* **2001**, *42*, 8647–8655. [[CrossRef](#)]
58. Hammami, A.; Spruiell, J.E.; Mehrotra, A.K. Quiescent nonisothermal crystallization kinetics of isotactic polypropylenes. *Polym. Eng. Sci.* **1995**, *35*, 797–804. [[CrossRef](#)]
59. Huang, Y.; Liu, H.; He, P.; Yuan, L.; Xiong, H.; Xu, Y.; Yu, Y. Nonisothermal crystallization kinetics of modified bamboo fiber/PCL composites. *J. Appl. Polym. Sci.* **2010**, *116*, 2119–2125. [[CrossRef](#)]
60. Zhu, B.-D.; Zhang, J.-Y.; Lin, C.-H.; Chen, H.-L.; Wang, J. Nonisothermal crystallization kinetics of ethylene vinyl alcohol copolymer with poly (oxypropylene) diamine intercalated montmorillonite. *J. Macromolecul. Sci. Part B* **2018**, *57*, 333–347. [[CrossRef](#)]
61. Avrami, M. Kinetics of phase change. I General theory. *J. Chem. Phys.* **1939**, *7*, 1103–1112. [[CrossRef](#)]
62. Wang, Y.; Rodriguez-Perez, M.A.; Reis, R.L.; Mano, J.F. Thermal and thermomechanical behaviour of polycaprolactone and starch/polycaprolactone blends for biomedical applications. *Macromol. Mater. Eng.* **2005**, *290*, 792–801. [[CrossRef](#)]
63. Huang, H.; Gu, L.; Ozaki, Y. Non-isothermal crystallization and thermal transitions of a biodegradable, partially hydrolyzed poly (vinyl alcohol). *Polymer* **2006**, *47*, 3935–3945. [[CrossRef](#)]

64. Kalkar, A.; Deshpande, A. Kinetics of isothermal and non-isothermal crystallization of poly (butylene terephthalate)/liquid crystalline polymer blends. *Polym. Eng. Sci.* **2001**, *41*, 1597–1615. [[CrossRef](#)]
65. Kissinger, H.E. Variation of peak temperature with heating rate in differential thermal analysis. *J. Res. Natl. Bur. Stand.* **1956**, *57*, 217–221. [[CrossRef](#)]
66. Amin, A.; Sarkar, R.; Moorefield, C.N.; Newkome, G.R. Preparation of different dendritic-layered silicate nanocomposites. *Polym. Eng. Sci.* **2013**, *53*, 2166–2174. [[CrossRef](#)]
67. Yang, Z.; Peng, H.; Wang, W.; Liu, T. Crystallization behavior of poly (ϵ -caprolactone)/layered double hydroxide nanocomposites. *J. Appl. Polym. Sci.* **2010**, *116*, 2658–2667. [[CrossRef](#)]